Small-Signal Stability Analysis of a DFIG-Based Wind Power System Under Different Modes of Operation

Yateendra Mishra, *Member, IEEE*, S. Mishra, *Senior Member, IEEE*, Fangxing Li, *Senior Member, IEEE*, Zhao Yang Dong, *Senior Member, IEEE*, and Ramesh C. Bansal, *Senior Member, IEEE*

***Abstract*—This paper focuses on the super/subsynchronous operation of the doubly fed induction generator (DFIG) system. The impact of a damping controller on the different modes of operation for the DFIG-based wind generation system is investigated. The coordinated tuning of the damping controller to enhance the damping of the oscillatory modes using bacteria foraging technique is presented. The results from eigenvalue analysis are presented to elucidate the effectiveness of the tuned damping controller in the DFIG system. The robustness issue of the damping controller is also investigated.**

***Index Terms*—Bacteria foraging (BF), control, coordinated tuning, damping controller, Doubly fed induction generator (DFIG), small-signal stability, subsynchronous operation, supersynchronous, wind turbine (WT).**

I. Introduction

WIND energy is one of the fastest growing industries worldwide. Increasing power generation from renewable sources, such as wind, would help in reducing carbon emissions, and hence, minimize the effect on global warming. Increasing steps have been taken by the various utilities/states across the world to achieve the aforementioned goal. Most of the states in the U.S. have Renewable Portfolios Standard (a state policy aiming at obtaining certain percentage of the their power form renewable energy sources by certain date) ranging from 10% to 20% of total capacity by 2020 [1]. This increasing penetration of renewable sources of energy, in particular, wind energy conversion systems (WECS), in the conventional power system has put tremendous challenge to the power system operators/planners, who have to ensure the reliable and secure grid operation. As power generation from WECS is significantly increasing, it is of paramount importance to study the effect of wind integrated power systems on overall system stability.

Manuscript received December 29, 2008; revised June 16, 2009. First published November 3, 2009; current version published November 20, 2009. Paper no. TEC-00519-2008.

Y. Mishra is with the Midwest ISO, Carmel, IN 46082-4202 USA (e-mail: ymishra@midwestiso.org).

S. Mishra is with the Indian Institute of Technology Delhi, New Delhi 110016, India (e-mail: sukumar@ee.iitd.ac.in).

F. Li is with the University of Tennessee, Knoxville, TN 37996 USA (e-mail: fli6@utk.edu).

Z. Y. Dong is with the Department of Electrical Engineering, Hong Kong Polytechnic University, Kowloon, Hong Kong (e-mail: eezydong@polyu.edu.hk).

R. C. Bansal is with the University of Queensland, Brisbane, Qld. 4072, Australia (e-mail: rcbansal@ieee.org).

Color versions of one or more of the figures in this paper are available online at http://ieeexplore.ieee.org.

Digital Object Identifier 10.1109/TEC.2009.2031498

The doubly fed induction generator (DFIG) has been popular among various other techniques of wind power generation, because of its higher energy transfer capability, low investment, and flexible control [2]. DFIG is different from the conventional induction generator in a way that it employs a series voltage-source converter to feed the wound rotor. The feedback converters consist of a rotor-side converter (RSC) and a grid-side converter (GSC). The control capability of these converters give DFIG an additional advantage of flexible control and stability over other induction generators.

The decoupled control of DFIG has the following controllers, namely $P_{\rm ref}$, $V_{\rm sref}$, $V_{\rm dcref}$, and $q_{\rm cref}$. These controllers are required to maintain maximum power tracking, stator terminal voltage, dc voltage level, and GSC reactive power level respectively. The coordinated tuning of these controllers by hit-and-trial method is a cumbersome job. The coordinated tuning using particle swarm optimization (PSO) has been proposed [3], [4]. However, the damping of low-frequency oscillatory modes were not given due importance.

The impact of wind generation on the oscillatory modes is presented in [5]–[8]. The auxiliary control loop for oscillation damping that adjusts the active power command to damp the interarea oscillation is proposed in [5] and [6]. Moreover, a power system stabilizer (PSS) using a speed deviation is proposed in [8]. It is reported that the presence of the PSS in the DFIG system improves the damping of the oscillations in the network. Nevertheless, it is very important to optimize the controller parameters of the PSS to achieve the best performance. However, the coordinated tuning of these controllers is not presented. Moreover, it is necessary to study the impact of these damping controllers under super/subsynchronous mode of operation.

In this paper, the auxiliary signal derived from ω_r is added to the rotor phase angle control to enhance the low-frequency damping of the system. This simple proportional–integral (PI) controller is called damping controller. Moreover, all the DFIG controllers, namely $P_{\rm ref}$, $V_{\rm sref}$, $V_{\rm dcref}$, and $q_{\rm cref}$ are implemented in this paper. Hence, the coordinated effect of these controllers on the system damping is examined. The effectiveness of damping controller under super/subsynchronous modes of operation is also investigated. The issue of robustness in the performance of the damping control is discussed.

The contribution of this paper are to: 1) study the impact of tuned damping controller on the electromechanical modes; 2) study its impact under super/subsynchronous mode of operation; and 3) propose the optimally tuned damping controller which

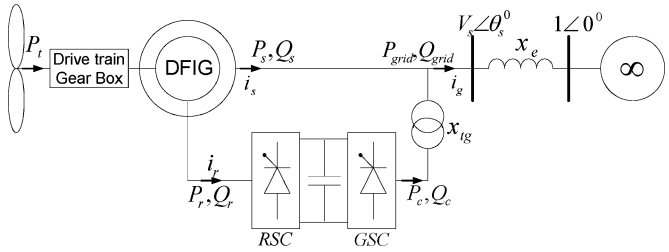

Fig. 1. DFIG system.

is effective under variable operating condition. This paper is structured as follows. Section II presents the modeling of the DFIG system. The detailed control methodology is discussed in Section III with special emphasis on damping controller. Section IV describes the bacteria foraging (BF) algorithm for the optimization of the controllers parameters. Section V discusses simulation and results followed by conclusions in Section VI.

II. Modeling of DFIG

The grid-connected single machine infinite bus (SMIB) system is considered and is shown in Fig. 1. The stator and rotor voltages of the doubly excited DFIG are supplied by the grid and the power converters, respectively.

Simulation of the realistic response of the DFIG system requires the modeling of the controllers in addition to the main electrical and mechanical components. The components considered includes turbine, drive train, generator, and the back-to-back converter system. These components are well established in the literature [9]; however, for the sake of completeness of the paper, they are introduced in brief as shown later.

A. Turbine and Drive Train

The mechanical power input to the WT is considered as constant, i.e., the blade pitch angle do not change during the period of study. In this paper, the two-mass drive train model [10] is considered and the dynamics can be expressed by the following differential equations [11]:

$$2H_t\frac{d\omega_t}{dt} = T_m - T_{\rm sh} \tag{1}$$

$$\frac{1}{\omega_{\rm elb}}\frac{d\theta_{tw}}{dt} = \omega_t - \omega_r \tag{2}$$

$$2H_g\frac{d\omega_r}{dt} = T_{\rm sh} - T_e \tag{3}$$

where $T_e = P_s/\omega_s$ is the electrical torque, $T_{\rm sh} = K_{\rm sh}\theta_{tw}$ is the shaft torque, H_t is the inertia constant of turbine, H_g is the inertia constant of the generator, θ_{tw} is the shaft twist angle, ω_t is the wind turbine (WT) angular speed, ω_r is the generator angular speed, ω_s is the synchronous speed, $\omega_{\rm elb}$ is the electrical base speed, and $K_{\rm sh}$ is the shaft stiffness.

B. Generator

The most common way of representing DFIG for the purpose of simulation and control is in terms of direct and quadrature axes (dq axes) quantities, which form a reference frame that rotates synchronously with the stator flux vector [9]. The various variables are defined as: $e'_{qs} = K_{mrr}\omega_s\psi_{dr}$, $e'_{ds} = -K_{mrr}\omega_s\psi_{qr}$, $L'_s = L_{ss} - (L_m^2/L_{rr})$, $T_r = L_{rr}/R_r$, $K_{mrr} = L_m/L_{rr}$, $\omega_e = \omega_{\rm elb}\omega_s$, $R_2 = K_{mrr}^2 R_r$, and $R_1 = R_s + R_2$. Here, L_{ss} is the stator self-inductance, L_{rr} is the rotor self inductance, L_m is the mutual inductance between rotor and stator, R_r is the rotor resistance, and R_s is the stator resistance.

For balanced and unsaturated conditions, the corresponding p.u. DFIG model can be expressed as [9]

$$\frac{\omega_s L'_s}{\omega_e}\frac{di_{qs}}{dt} = -R_1 i_{qs} + \omega_s L'_s i_{ds} + \frac{\omega_r}{\omega_s}e'_{qs} - \frac{1}{T_r\omega_s}e'_{ds}\cdots \cdots - v_{qs} + K_{mrr}v_{qr} \tag{4}$$

$$\frac{\omega_s L'_s}{\omega_e}\frac{di_{ds}}{dt} = -R_1 i_{ds} - \omega_s L'_s i_{qs} + \frac{\omega_r}{\omega_s}e'_{ds} + \frac{1}{T_r\omega_s}e'_{qs}\cdots \cdots - v_{ds} + K_{mrr}v_{dr} \tag{5}$$

$$\frac{1}{\omega_e}\frac{de'_{qs}}{dt} = R_2 i_{ds} - \frac{1}{T_r\omega_s}e'_{qs} + \left(1 - \frac{\omega_r}{\omega_s}\right)e'_{ds} - K_{mrr}v_{dr} \tag{6}$$

$$\frac{1}{\omega_e}\frac{de'_{ds}}{dt} = -R_2 i_{qs} - \frac{1}{T_r\omega_s}e'_{ds} - \left(1 - \frac{\omega_r}{\omega_s}\right)e'_{qs} + K_{mrr}v_{qr} \tag{7}$$

where e'_{ds} and e'_{qs} are d- and q-axis voltages behind transient reactance, respectively, ψ_{dr} and ψ_{qr} are d- and q-axis rotor fluxes, respectively, and i_{ds} and i_{qs} are d- and q-axis stator currents, respectively.

C. Converter Model

The converter model in DFIG system comprises of two pulsewidth modulation invertors connected back to back via a dc link. The RSC and the GSC act as a controlled voltage sources. The RSC injects an ac voltage at slip frequency to the rotor, whereas the GSC injects an ac voltage at power frequency to the grid and maintains the dc-link voltage constant. The power balance equation for the converter model can be written as

$$P_r = P_g + P_{\rm dc} \tag{8}$$

where P_r, P_g, and $P_{\rm dc}$ are the active power at RSC, GSC, and dc link, respectively, which can be expressed as follows:

$$P_r = v_{dr}i_{dr} + v_{qr}i_{qr} \tag{9}$$

$$P_g = v_{dg}i_{dg} + v_{qg}i_{qg} \tag{10}$$

$$P_{\rm dc} = v_{\rm dc}i_{\rm dc} = Cv_{\rm dc}\frac{dv_{\rm dc}}{dt} \tag{11}$$

where v_{ds} and v_{qs} are d- and q-axis stator voltages, respectively, i_{dr} and i_{qr} are d- and q-axis rotor currents, respectively, i_{dg} and i_{qg} are d- and q-axis currents of the GSC, respectively, v_{dg} and v_{qg} are d- and q-axis voltages of the GSC, respectively, v_{dr} and v_{qr} are d- and q-axis rotor voltages, respectively, $v_{\rm dc}$ and $i_{\rm dc}$ are the voltage and current of the dc-link capacitor, respectively,

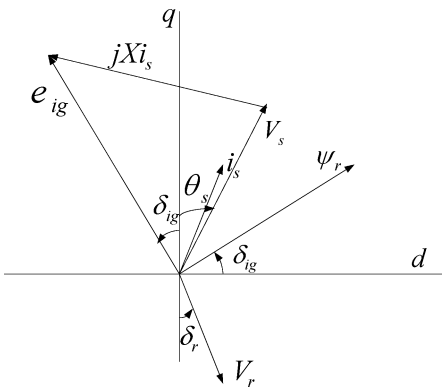

Fig. 2. Phasor diagram illustrating the operation of DFIG system [8].

and C is the capacitance of the dc capacitor. The direction of the currents and power flow is shown in Fig 1.

The details of converter controllers are elaborated in the following section.

III. Controllers for DFIG

This section describes the controllers used for the DFIG system. As mentioned earlier, there are two back-to-back converters; hence, we need to control these two converter sides. Primarily, these controller are known as RSC and GSC controllers. This section also introduces a new auxiliary control signal that is added to the angle control in the RSC to enhance the damping. This is known as damping control.

A. RSC Controllers

The phasor diagram in Fig. 2 describes the control scheme [based on flux magnitude angle control (FMAC)], for the RSC controller.

The magnitude of the e_{ig}, internally generated voltage vector in the stator, depends on the magnitude of the rotor flux vector ψ_r. This flux can be controlled by V_r, the rotor voltage. The angle δ_{ig}, between the voltage vectors e_{ig} and V_s (stator terminal voltage and hence q-axis of the reference frame), is determined by the power output of the DFIG. Since vector e_{ig} is orthogonal to ψ_r, the angle between d-axis and ψ_r is also given by δ_{ig}. The adjustment of the magnitude of the rotor voltage vector, $|V_r|$ and its phase angle, δ_r, is employed for the control of terminal voltage and electrical power, respectively [8].

The configuration of the feedback controllers for the DFIG system is shown in Fig. 3. The RSC controller is shown in Fig. 3(a). One part aims at controlling the active power so as to track the $P_{\rm ref}$, while the second part is to maintain the terminal voltage.

$P_{\rm ref}$ is determined by the WT power speed characteristic ($C_p - \lambda$ curve) for maximum power extraction [10]. Under normal operating condition, the active power set point $P_{\rm ref}$ for the RSC is defined by the maximum power tracking point, which is a function of optimal generation speed. Mathematically, the aforementioned concept can be expressed by the set of differential

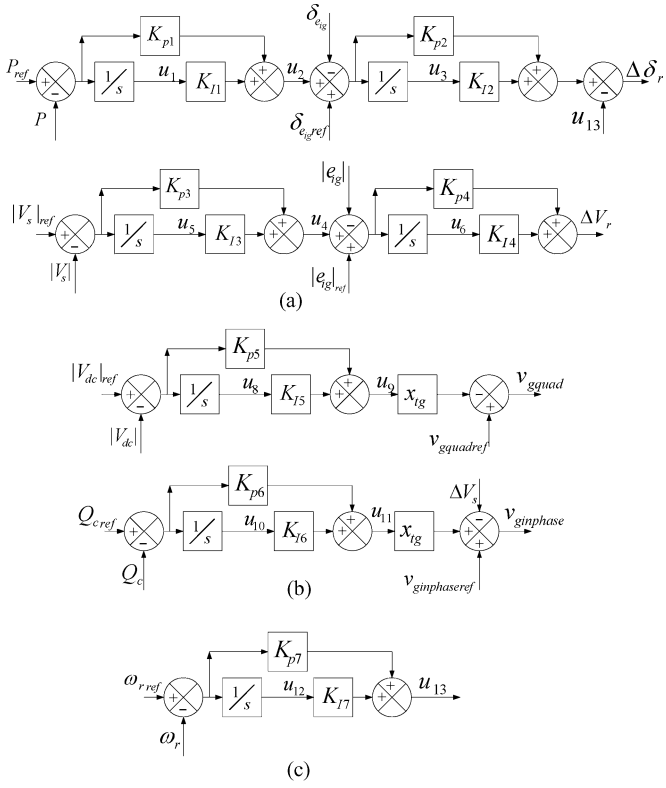

Fig. 3. Control scheme for the DFIG system. (a) RSC. (b) GSC. (c) Damping controller.

equations as follows:

$$\frac{du_1}{dt} = P_{\rm ref} - P \tag{12}$$

$$u_2 = K_{p1}(P_{\rm ref} - P) + K_{I1}u_1 \tag{13}$$

$$\frac{du_3}{dt} = (\delta_{e_{ig}\,\rm ref} + u_2 - \delta_{e_{ig}}) \tag{14}$$

$$u_4 = K_{p3}(V_{\rm sref} - V_s) + K_{I3}u_5 \tag{15}$$

$$\frac{du_5}{dt} = V_{\rm sref} - V_s \tag{16}$$

$$\frac{du_6}{dt} = (|e_{ig}|_{\rm ref} + u_4 - |e_{ig}|) \tag{17}$$

$$\Delta\,|V_r| = K_{p4}(|e_{ig}|_{\rm ref} + u_4 - |e_{ig}|) + K_{I4}u_6 \tag{18}$$

$$\frac{du_{12}}{dt} = \omega_{r\rm ref} - \omega_r \tag{19}$$

$$u_{13} = K_{p7}(\omega_{r\rm ref} - \omega_r) + K_{I7}u_{12} \tag{20}$$

$$\Delta\delta_r = (K_{p2}(\delta_{e_{ig}\,\rm ref} + u_2 - \delta_{e_{ig}}) + K_{I2}u_3) - u_{13} \tag{21}$$

where K_{pi} and K_{Ii} are the proportional and integral gain constant respectively for ith PI controller. The internal generated voltage vector, e_{ig} is given by, $|e_{ig}| = \sqrt{e_{ds}'^2 + e_{qs}'^2}$, and the angle is defined as $\delta_{e_{ig}} = \tan^{-1}\left(e_{ds}'/e_{qs}'\right)$.

B. GSC Controllers

The GSC controller scheme is represented in Fig. 3(b). The reference signal for the dc voltage $V_{\rm dcref}$ is set to a constant value independent of the wind speed, and $V_{\rm dc}$ is regulated by the following equation:

$$\frac{dV_{\rm dc}}{dt} = \frac{1}{V_{\rm dc}C}\left(v_{dr}i_{dr} + v_{qr}i_{qr} - v_{dg}i_{dg} - v_{qg}i_{qg}\right) \quad (22)$$

$$\frac{du_8}{dt} = V_{\rm dcref} - V_{\rm dc} \quad (23)$$

$$u_9 = K_{P5}(V_{\rm dcref} - V_{\rm dc}) + K_{I5}u_8. \quad (24)$$

The reactive power set point $q_{\rm cref}$ is set to zero in order to reduce the GSC power rating. This implies that GSC only exchanges active power with the grid, and hence, the reactive power transmission to the grid by DFIG is only through the stator

$$\frac{du_{10}}{dt} = q_{\rm cref} - q_c \quad (25)$$

$$u_{11} = K_{P6}(q_{\rm cref} - q_c) + K_{I6}u_{10}. \quad (26)$$

The inphase and quadrature component of the GSC voltage is modified by

$$v_{g\rm inphase} = v_{g\rm inphaseref} + u_{11}x_{tg} - (V_{s\rm ref} - V_s) \quad (27)$$

$$v_{g\rm quad} = v_{g\rm quadref} - u_9 x_{tg} \quad (28)$$

where $v_{g\rm inphaseref} = V_s + i_{cg\rm quadref} * x_{tg}$ and $v_{g\rm quad} = i_{cg\rm inphaseref} * x_{tg}$, and x_{tg} is the three-winding transformer reactance between GSC and the stator terminal. $i_{cg\rm inphaseref}$ and $i_{cg\rm quadref}$ are the inphase and quadrature component of GSC current to the stator terminal voltage defined as $i_{cg\rm inphaseref} = P_r/V_s$ and $i_{cg\rm quadref} = (v_{ds} * i_{qg} - v_{qs} * i_{dg})/V_s$.

The corresponding GSC control scheme is implemented in this paper.

C. Damping Controller

Damping controller is employed in the RSC by (20), as shown in Fig. 3(c). The auxiliary signal u_{13} is added to the angle control of the RSC controller to enhance the damping of low-frequency angular oscillations. The auxiliary signal helps in increasing the damping torque by controlling the angular position of the rotor flux vector with respect to the stator flux vector.

The change in the wind speed is sensed by a sensor and then "$\omega_{r\rm ref}$" is determined by the maximum power tracking from $C_p(\lambda, \beta)$ curve. For a constant "λ," the ratio, ω_r/V_w, is constant, as a result

$$\begin{aligned}\frac{\omega_{r1\rm ref}}{V_{w1}} = \frac{\omega_{r2\rm ref}}{V_{w2}} &\Rightarrow \frac{\omega_{r1\rm ref}}{\omega_{r2\rm ref}} = \frac{V_{w1}}{V_{w2}} \\ &\Rightarrow \frac{(1-s_1)\omega_s}{(1-s_2)\omega_s} = \frac{V_{w1}}{V_{w2}} \\ &\Rightarrow \frac{(1-p_{r1}/p_{s1})}{(1-p_{r2}/p_{s2})} = \frac{V_{w1}}{V_{w2}} \end{aligned} \quad (29)$$

where s denotes the slip, p_r and p_s are rotor and stator power before losses. However, as the losses are very small, the values of p_r and p_s can be approximately equal to P_r and P_s. This is important as the application of the damping controller in DFIG should also ensure that the maximum power is extracted from the wind.

Thus, in summary, the state equations of the DFIG are (1)–(7), while RSC and GSC controller state equations are (12), (14), (16), (17), (22), (23), and (25). The damping controller state equation is (19). Hence, there are total 15 states of the DFIG system including the damping controller.

IV. BF for the Optimal Control of DFIG System

The idea of BF is based on the fact that, natural selection tends to eliminate animals with poor foraging strategies and favor the propagation of genes of those animals that have successful foraging strategies since they are more likely to enjoy reproductive success. After many generations, poor foraging strategies are either eliminated or reshaped into good ones. The *Escherichia coli* bacteria that are present in our intestines also undergo a foraging strategy. The control of these bacteria is basically governed by four processes, namely chemotaxis, swarming, reproduction, elimination, and dispersal [12].

A. Chemotaxis

This process is achieved through swimming and tumbling. Depending upon the rotation of the flagella in each bacterium it decides whether it should move in a predefined direction (swimming) or an altogether different direction (tumbling), in the entire lifetime of the bacterium. To represent a tumble, a unit length random direction, say $\phi(j)$, is generated; this will be used to define the direction of movement after a tumble. In particular

$$\theta^i(j+1,k,l) = \theta^i(j,k,l) + {\rm Cl}(i)\phi(j) \quad (30)$$

where $\theta^i(j,k,l)$ represents the ith bacterium at jth chemotactic kth reproductive and lth elimination and dispersal step. ${\rm Cl}(i)$ is the size of the step taken in the random direction specified by the tumble (run length unit).

B. Swarming

During the process of reaching toward the best food location it is always desired that the bacterium which has searched optimum path should try to attract other bacteria so that they reach the desired place more rapidly. Swarming makes the bacteria congregate into groups and hence move as concentric patterns of groups with high bacterial density. Mathematically, swarming can be represented by

$$\begin{aligned} J_{cc}(\theta, P(j,k,l)) &= \sum_{i=1}^{S} J_{cc}^i\left(\theta, \theta^i(j,k,l)\right) \\ &= \sum_{i=1}^{S}\left[-d_{\rm attract}\exp\left(-\omega_{\rm attract}\sum_{m=1}^{p}(\theta_m - \theta_m^i)^2\right)\right] \\ &+ \sum_{i=1}^{S}\left[h_{\rm repellant}\exp\left(-\omega_{\rm repellant}\sum_{m=1}^{p}(\theta_m - \theta_m^i)^2\right)\right] \end{aligned} \quad (31)$$

where $J_{cc}(\theta, P(j,k,l))$ is the cost function value to be added to the actual cost function to be minimized to present a time varying cost function. Then, $J_{sw} = J + J_{cc}$ is calculated, where "J" is the actual cost function to be minimized, "S" is the total number of bacteria, "p" is the number of parameters to be optimized that are present in each bacterium, "θ_m" is the global best parameter available during that iteration, "$P(j,k,l)$)" is the last value of θ stored for the next iteration, d_{attract}, ω_{attract}, $h_{\text{repellant}}$, and $\omega_{\text{repellant}}$ are different coefficients that are to be chosen judiciously, d_{attract} is the depth of the attractant released by the cell and sets the magnitude of secretion of attractant by a cell, and ω_{attract} is the width of the attractant signal and determines the chemical cohesion signal diffusion (smaller value makes it diffuse more). Here, $h_{\text{repellant}}$ is the height of the repellant effect and $\omega_{\text{repellant}}$ is the measure of the width of the repellant that controls the tendency to repel other cells.

The magnitude of d_{attract} and $h_{\text{repellant}}$ should be same [13]. It is so that there is no penalty added to the cost function when the bacterial population converges, i.e., J_{cc} of (27) will be 0. Their numerical value should be decided based on the required variation in the magnitude of the actual cost function "J" to obtain a satisfactory result. The value of ω_{attract} and $\omega_{\text{repellant}}$ should be such that if the euclidian distance between bacteria is large, the penalty J_{cc} is large.

C. Reproduction

The least healthy bacteria die and the all other healthier bacteria split into two bacteria, which are placed in the same location. This makes the population of bacteria constant. Instead of taking the average value of all the chemotactic cost functions, the minimum value is selected for deciding the health of the bacteria [14]. Mathematically, for particular kth and lth, the health of the ith bacteria would be given by, $J^i_{\text{health}} = \min_{j\varepsilon\{1,2,\ldots,N_c\}} \{J_{sw}(i,j,k,l)\}$.

D. Elimination and Dispersal

It is possible that in the local environment the life of a population of bacteria changes either gradually (e.g., via consumption of nutrients) or suddenly due to some other influence. Events can occur such that all the bacteria in a region are killed or a group is dispersed into a new part of the environment. They have the effect of possibly destroying the chemotactic progress, but they also have the effect of assisting in chemotaxis, since dispersal may place bacteria near good food sources. From a broad perspective, elimination and dispersal are parts of the population-level long-distance motile behavior. It helps in reducing the behavior of stagnation (i.e. being trapped in a premature solution point or local optima) often seen in such parallel search algorithms. This section is based on the work in [15]. The detailed mathematical derivations as well as theoretical aspect of this new concept are presented in [12]–[17].

In this paper, optimization using BF scheme is carried out to find the optimal controller parameters of the DFIG system. The algorithm is presented in the flowchart, as shown in Fig. 4.

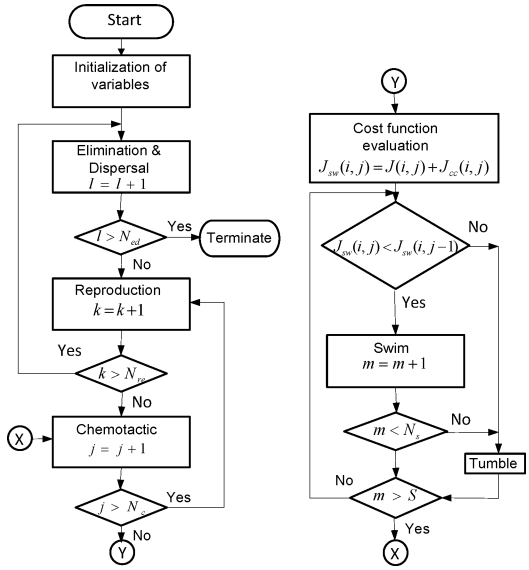

Fig. 4. Flowchart summarizing the BF algorithm for the optimization of controller parameters.

V. Simulation and Results

The aforementioned optimization technique is applied to a SMIB DFIG system. The DFIG system with controllers can be represented by the set of differential and algebraic equations (DAEs) as

$$\dot{x} = f(x,y,u)$$
$$0 = g(x,y,u) \tag{32}$$

where x, y, and u are the vectors of DFIG state, algebraic and control variables respectively. The state vector is defined by

$$x = [i_{qs}, i_{ds}, e'_{qs}, e'_{ds}, \omega_r, \theta_{wt}, \ldots$$
$$\ldots, \omega_t, v_{\text{dc}}, u_1, u_3, u_5, u_6, u_8, u_{10}, u_{12}]^T. \tag{33}$$

Linearizing the previous DAE about an operating point (x_0, y_0, u_0) (which is obtained by the load flow at a particular wind speed), the system matrix A_{sys} can be calculated as follows:

$$\Delta \dot{x} = A_{\text{sys}} \Delta x. \tag{34}$$

The parameters of the DFIG system is given in Appendix.

A. Objective Function

The parameters of DFIG controllers are selected so as to minimize the following objective function:

$$J = \frac{1}{(\min\limits_{\forall i} \zeta_i)} \tag{35}$$

where ζ_i is the damping ratio of the ith eigenvalue of the system. This objective function makes sure that the minimum damped eigenvalue is heavily damped and the system small-signal stability is ensured. The controller parameters are optimized with the previous objective function and the performance of the algorithm is shown in Fig. 7 in the Appendix.

TABLE I
DIFFERENT MODES OF OPERATION OF DFIG-BASED WT SYSTEM

Mode of Operation (Wind Speed)	Power from Stator (P_s)	Power from Rotor (P_r)	Total Power ($P_t = P_r + P_s$)
Normal Mode (8 m/sec)	1.1562	-0.024	1.1322
Super-synchronous (10 m/sec)	1.8017	0.4096	2.2113
Sub-synchronous (6 m/sec)	0.6565	-0.1789	0.4776

TABLE II
SELECTED EIGENVALUES OF THE WT SYSTEM WITHOUT ANY CONTROLLERS AT WIND SPEED OF 8 M/S

Mod No.	Eigenvalue λ	Freq (Hz)	Damp (%)	Participation factor (%)
1	-38.22±j504.77	80.33	7.55	$i_{qs}(49.2\%), i_{ds}(48.2\%), e^{'}_{ds}(1.2\%)$
2	-4.80±j53.41	8.5	8.95	$e^{'}_{ds}(47.6\%), \omega_r(47.9\%), i_{ds}(1.9\%)$
3	-0.26±j3.36	0.53	7.9	$\theta_{tw}(48.03\%), \omega_t(49.7\%), e^{'}_{qs}(1.96\%)$

B. Performance of DFIG-Based WT System Under Different Modes of Operation

It is important to emphasize the steady-state operation of the DFIG-based WT system under different modes of operation. Based on the average wind speed in the particular area, the WT (blade radius) can be designed to operate DFIG near the synchronous speed. The near synchronous speed would be desired by the manufacturer so as to extract maximum power from the stator and hence put less burden on rotor convertors. This would help the rotor current to not exceed RSC and GSC thermal rating in the event of wind speed variation. Hence, this would enhance the life cycle of the convertors. From the operation point of view, the additional rotor power at increased wind speed would give some reserve which can be added to the grid.

With the given WT rating (in the Appendix), DFIG operates at supersynchronous mode when the wind speed (V_w) is more than 8 m/s and at subsynchronous mode at lower wind speeds. Table I shows different modes of operation of the given DFIG WT system. At supersynchronous mode, the power is supplied by stator as well as rotor, whereas rotor absorbs power at subsynchronous mode of operation. The power coming in to the RSC and going out of GSC is considered positive, as shown in Fig 1.

C. Need of Damping Controller

The eigenvalues of the WT system without any control at wind speed of 8 m/s is shown in Table II. The system looks stable with well damped eigenvalues. The first mode is stator or electrical mode and the second is electromechanical mode, which can be identified by looking at the participation factors. As electrical state (e_{ds}) and mechanical state (ω_r) participates in the second mode, hence this mode is electromechanical mode. The stator mode has the lowest damping ratio but its frequency is high and hence out of the range of interest. The low-frequency mode, i.e mechanical mode (0.53 Hz) is well damped. However, the application of controllers (necessary to enhance the performance of the DFIG system) affects its damping, as shown in Tables III–V.

Initially, the $P_{\rm ref}$, $V_{\rm sref}$, $V_{\rm dcref}$, and $q_{\rm cref}$ are implemented in the DFIG system. The parameters of these four controllers are optimized using BF algorithm for a wind speed of 8 m/s (normal mode of operation). It is observed from Table III that mode# 3 is unstable at higher wind speed (supersynchronous mode of operation). With the implementation of the optimized damping controller (using BF and keeping all other controller parameter as constant), the system is stable. The further detailed discussion can be found in [18].

However, the closer look at the eigenvalues gives a new dimension to the whole problem. The damping controller enhances the damping at normal and supersynchronous mode of operation, but at lower wind speeds (subsynchronous operation), mode# 2 becomes unstable. This mode remains unstable even after the implementation of damping controller, as shown in Table III. This requires further investigation as to how this mode is excited and what can be done to make the system stable.

The Wind speed is seldom constant and hence there is a need for a robust damping controller which can perform well under various operating conditions. Therefore, to further investigate the impact of damping controller at different operating conditions, the DFIG system is studied for supersynchronous and subsynchronous modes of operation.

D. Optimal Tuning of DFIG Controllers

The robust performance of DFIG controllers is desired at all modes (normal and super/subsynchronous) to ensure the stable operation of the WT under stochastically varying wind speed. Hence, it is necessary to find the optimal parameters of all the controllers (including damping controller) for the stable operation under changing wind speeds. Usually, the wind speed varies in the range of 6–14 m/s. However, these extreme wind speeds are rare and hence the speed of 8 m/s is selected for the near synchronous or normal mode of operation (it depends on turbine manufacturer and the average wind speed selection). For the optimal performance, controllers should be optimized at the speed near to the rated/normal speed. Therefore, the DFIG controllers are optimized at three different wind speeds (V_w), i.e., 8 m/s (normal), 8.5 m/s (supersynchronous), and 7 m/s (subsynchronous). This is shown in Tables III–V.

When the controllers are optimized for $V_w = 8$ m/s, the system is stable for normal ($V_w = 8$ m/s) and supersynchronous ($V_w > 8$ m/s) mode of operation. However, at subsynchronous ($V_w < 8$ m/s) mode of operation, mode# 2 becomes unstable, as shown in Table III. It is interesting to observe that the damping controller still works well at this mode of operation, as mode# 3 is stable with damping controller. However, mode# 2 has become unstable because the participation of the mechanical state (ω_r) has been reduced and that of electrical states (e'_{ds}, e'_{qs}) have increased at the subsynchronous mode of operation, which can be seen from Table III. This suggests that the system is not small-signal stable at subsynchronous mode of operation, if the

TABLE III
SELECTED EIGENVALUES OF THE WT SYSTEM

	Without Damping Controller					With Damping Controller				
Mode of Operation (Wind Speed)	Mod No.	Eigenvalue λ	Freq (Hz)	Damp (%)	Participation factors	Mod No.	Eigenvalue λ	Freq (Hz)	Damp (%)	Participation factors
Normal operation (8 m/sec)	1	-42.11±j509	81.1	8.22	i_{qs}, i_{ds}	1	-42.05±j509	81.1	8.22	i_{qs}, i_{ds}
	2	-15.03±j64.6	10.2	22.6	e'_{ds}, ω_r	2	-13.93±j64.9	10.3	20.9	e'_{ds}, ω_r
	3	**-0.98±j3.53**	**0.56**	**26.9**	θ_{tw}, e'_{qs}	**3**	**-0.97±j3.34**	**0.53**	**27.8**	ω_t, θ_{tw}
	4	-0.014±j0.04	0.006	31.8	u_1, u_8	4	-0.714±j0.319	0.05	91.2	u_{12}, u_8
Super-Synchronous operation (10 m/sec)	1	-26.93±j469	74.7	5.7	i_{qs}, i_{ds}	1	-27.50±j468	74.6	5.85	i_{qs}, i_{ds}
	2	-48.4±j261	41.56	18.2	e'_{ds}, e'_{qs}, i_{ds}	2	-45.73±j261	41.65	17.2	e'_{ds}, e'_{qs}, i_{ds}
	3	**0.61±j11.1**	**1.76**	**-5.4**	θ_{tw}, e'_{qs}	**3**	**-1.35±j12.82**	**2.04**	**10.52**	$\omega_r, \theta_{tw}, e'_{qs}$
	4	-0.46±j0.259	0.04	87.1	V_{dc}, u_8	4	-0.41±j1.82	0.29	21.8	ω_t, u_8
	5	-0.12±j0.04	0.007	93.7	u_3, u_1	5	-0.54±j0.016	0.002	99.9	u_6, u_8
Sub-Synchronous operation (6 m/sec)	1	-50.33±j590	93.9	8.4	i_{ds}, i_{qs}	1	-49.21±j590	93.9	8.3	i_{qs}, i_{ds}
	2	**3.82±j219**	**34.9**	**-1.7**	e'_{qs}, e'_{ds}	**2**	**4.82±j219**	**34.8**	**-2.2**	e'_{ds}, e'_{qs}
	3	**-0.60±j11.1**	**1.76**	**5.4**	θ_{tw}, e'_{qs}	**3**	**-2.82±j12.7**	**2.03**	**21.5**	$\omega_r, \theta_{tw}, e'_{qs}$
	4	-0.18±j0.06	0.01	94.2	u_1, u_5	4	-0.46±j1.90	0.30	23.4	ω_t, u_8

The controllers are optimized at the rated wind speed of 8 m/s.

TABLE IV
SELECTED EIGENVALUES OF THE WT SYSTEM

	Without Damping Controller					With Damping Controller				
Mode of Operation (Wind Speed)	Mod No.	Eigenvalue λ	Freq (Hz)	Damp (%)	Participation factors	Mod No.	Eigenvalue λ	Freq (Hz)	Damp (%)	Participation factors
Normal operation (8 m/sec)	1	-39.50±j507	80.7	7.76	i_{qs}, i_{ds}	1	-39.06±j507	80.7	7.6	i_{qs}, i_{ds}
	2	-5.09±j53.55	8.52	9.4	e'_{ds}, ω_r	2	-4.87±j54.2	8.62	8.95	ω_r, e'_{ds}
	3	**-0.34±j3.67**	**0.58**	**9.42**	$\theta_{tw}, \omega_t, e'_{qs}$	**3**	**-0.41±j3.57**	**0.56**	**11.4**	ω_t, θ_{tw}
	4	-0.61±j4.94	0.78	12.3	u_8, V_{dc}	4	-0.61±j4.94	0.78	12.3	u_8, V_{dc}
	5	-0.02±j0.07	0.01	36.6	u_1, ω_t	5	-1.15±j1.00	0.16	75.4	u_6, u_{12}
Super-Synchronous operation (10 m/sec)	1	-30.69±j463	73.7	6.6	i_{qs}, i_{ds}	1	-38.85±j461	73.4	8.3	i_{qs}, i_{ds}
	2	-38.06±j149	23.8	24.64	$e'_{ds}, e'_{qs}, \omega_r$	2	-11.92±j164	26.1	7.25	$e'_{ds}, e'_{qs}, \omega_r$
	3	**1.56±j10.42**	**1.65**	**-14.8**	θ_{tw}, e'_{qs}	**3**	**-**	**-**	**-**	-
	4	-0.63±j5.06	0.80	12.3	V_{dc}, u_8	4	-0.54±j4.99	0.79	10.9	$V_{dc} u_8$
	5	-0.32±j0.574	0.09	49.3	ω_t, u_1, u_6	5	-0.86±j2.69	0.42	30.6	ω_t, θ_{tw}
Sub-Synchronous operation (6 m/sec)	1	-45.48±j557	88.8	8.12	i_{qs}, i_{ds}	1	-37.03±j557	88.8	6.6	i_{qs}, i_{ds}
	2	**2.21±j136**	**21.7**	**-1.6**	$e'_{qs}, e'_{ds}, \omega_r$	**2**	**14.97±j135**	**21.5**	**-11.6**	$e'_{qs}, e'_{ds}, \omega_r$
	3	**-1.61±j10.47**	**1.66**	**15.2**	θ_{tw}, e'_{qs}	**3**	**-**	**-**	**-**	-
	4	-0.56±j4.80	0.76	11.6	V_{dc}, u_8	4	-0.65±j4.87	0.77	13.3	V_{dc}, u_8
	5	-0.25±j0.198	0.03	78.7	ω_t, u_1, u_6	5	-0.85±j2.98	0.47	27.4	$\omega_t, \theta_{tw}, u_{12}$

The controllers are optimized at supersynchronous wind speed of 8.5 m/s.

controllers are optimized at near synchronous (normal) wind speed.

In the next step, the controller are optimized at wind speed (V_w) of 8.5 m/s. Again the system is unstable at subsynchronous mode of operation. This can be illustrated from Table IV. As shown in Table IV, the optimization at supersynchronous speed would help in eliminating the electromechanical mode (mode# 3). But on the downside, the system has an additional mode, mode# 4, associated with state $V_{\rm dc}$, voltage across the dc-link capacitor. This can have detrimental effect on the system stability if not properly damped. Moreover, it affects the convertor rating and therefore the oscillations of this kind should be damped if the controllers are optimized for this operating condition. Mode# 2 is still unstable at lower wind speeds (subsynchronous operation).

Lastly, the controllers are optimized at lower wind speeds, i.e., $V_w = 7$ m/s, and the eigenvalues of the system with the different controllers are shown in Table V. The system is stable for all the operating wind speeds. To further verify this, the controllers are optimized at $V_w = 7.5$ m/s and $V_w = 6.5$ m/s. Table VI summarizes the variation of mode# 2 when controllers are optimized at different wind speeds. It is observed that all the modes are stable if controllers are optimized at any subsynchronous speed. Again, the speed depends on the rating of the DFIG WT. For example, if the installed WT has near synchronous operation at $V_w = 8$ m/s, then the controllers can be designed at any subsynchronous speed ($V_w < 8$ m/s). This would ensure the stable performance of DFIG system across the wide range of wind speed from subsynchronous ($V_w < 8$ m/s) to supersynchronous ($V_w > 8$ m/s) mode of operation.

E. Super/Subsynchronous Mode of Operation

It is interesting to observe the change in the frequency of oscillations of different eigenmodes under super/subsynchronous operation of DFIG. The eigenvalues of the DFIG-based WT

TABLE V
SELECTED EIGENVALUES OF THE WT SYSTEM

	Without Damping Controller					With Damping Controller				
Mode of Operation (Wind Speed)	Mod No.	Eigenvalue λ	Freq (Hz)	Damp (%)	Participation factors	Mod No.	Eigenvalue λ	Freq (Hz)	Damp (%)	Participation factors
Normal operation (8 m/sec)	1	-39.13±j504	80.3	7.73	i_{qs}, i_{ds}	1	-39.08±j504	80.3	7.72	i_{qs}, i_{ds}
	2	-7.01±j56.14	8.93	12.4	ω_r, e'_{ds}	2	-6.16±j56.97	9.05	10.7	ω_r, e'_{ds}
	3	**-0.45±j3.38**	**0.53**	**13.3**	$\theta_{tw}, \omega_t, e'_{qs}$	**3**	**-0.43±j3.38**	**0.53**	**12.8**	ω_t, θ_{tw}
	4	-0.005±j0.03	0.005	14.3	u_1, u_3	4	-	-	-	-
Super-Synchronous operation (10 m/sec)	1	-37.14±j499	79.4	7.4	i_{qs}, i_{ds}	1	-37.53±j499	79.4	7.5	i_{qs}, i_{ds}
	2	-15.37±j140	22.4	10.8	$e'_{ds}, e'_{qs}, \omega_r$	2	-9.06±j141	22.5	6.3	$e'_{ds}, e'_{qs}, \omega_r$
	3	**0.86±j10.4**	**1.65**	**-8.2**	θ_{tw}, e'_{qs}	**3**	**-3.79±j9.56**	**1.52**	**36.8**	$\omega_r, \theta_{tw}, e'_{qs}$
	4	-0.02±j0.417	0.06	6.03	u_1, u_3, u_6	4	-0.58±j1.16	0.18	44.8	u_8, ω_t
Sub-Synchronous operation (6 m/sec)	1	-41.83±j505	80.5	8.2	i_{qs}, i_{ds}	1	-40.54±j506	80.5	7.9	i_{qs}, i_{ds}
	2	**-7.5±j146**	**23.3**	**5.1**	$e'_{qs}, e'_{ds}, \omega_r$	**2**	**-2.44±j145**	**23.2**	**1.6**	$e'_{qs}, e'_{ds}, \omega_r$
	3	**-1.65±j10.51**	**1.67**	**15.5**	θ_{tw}, e'_{qs}	**3**	**-9.51±j7.96**	**1.26**	**76.65**	$\omega_r, \theta_{tw}, e'_{qs}$
	4	-0.13±j0.23	0.03	51.2	u_1, u_5	4	-1.04±j1.17	0.18	66.2	ω_t, u_{15}

The controllers are optimized at subsynchronous wind speed of 7 m/s.

TABLE VI
BEHAVIOR OF MODE# 2 WHEN THE CONTROLLERS ARE OPTIMIZED AT DIFFERENT WIND SPEEDS

Mode of Operation (Wind Speed)	Wind Speed at which Controllers are optimized (m/sec)	Without Damping Controller			With Damping Controller		
		Eigenvalue (λ)	Freq (Hz)	Damp (%)	Eigenvalue (λ)	Freq (Hz)	Damp (%)
Normal operation (8 m/sec)	8.5	-5.10 ±j53.55	8.52	9.48	-4.87 ±54.21	8.63	8.96
	8.0	-15.04 ±j64.62	10.28	22.67	-13.93 ±64.95	10.34	20.98
	7.5	-10.95 ±j59.93	9.54	17.97	-10.17 ±60.51	9.63	16.57
	7.0	-7.02 ±j56.15	8.94	12.40	-6.17 ±56.98	9.07	10.76
	6.5	-5.33 ±j55.24	8.79	9.61	-5.18 ±55.33	8.81	9.33
Super-Synchronous operation (10 m/sec)	8.5	-38.07 ±j149.69	23.82	24.65	-11.93 ±j164.01	26.10	7.25
	8.0	-48.41 ±j261.14	41.56	18.23	-45.74 ±j261.70	41.65	17.22
	7.5	-28.16 ±j202.55	32.24	13.77	-25.29 ±j203.09	32.32	12.36
	7.0	-15.37 ±j140.75	22.40	10.86	-9.07 ±j141.71	22.55	6.38
	6.5	-14.17 ±j115.86	18.44	12.14	-12.61 ±j116.10	18.48	10.80
Sub-Synchronous operation (6 m/sec)	**8.5**	**2.21±j136.37**	**21.70**	**-1.62**	**14.98 ±j135.32**	**21.54**	**-11.00**
	8.0	**3.83±j219.40**	**34.92**	**-1.74**	**4.82±j219.13**	**34.88**	**-2.20**
	7.5	-1.77 ±j193.83	30.85	0.91	-0.19 ±j193.47	30.79	0.10
	7.0	-7.51 ±j146.49	23.31	5.12	-2.44 ±j145.79	23.20	1.67
	6.5	-6.84 ±j119.73	19.06	5.70	-5.58 ±j119.50	19.02	4.66

system is observed under super/subsynchronous mode of operation. It is observed that the frequency of mode# 2 has increased from $\sim$10 Hz (normal operation) to $\sim$40 Hz (super/subsynchronous operation) when the controllers are optimized at 8 m/s. Mode#2 has become electrical mode from electromechanical mode. This can be easily verified by the participation factor analysis, as shown in Table III. Moreover, when controllers are optimized for the wind speed of either 8.5 or 7 m/s, the frequency of mode# 2 changes to $\sim$20 Hz for super/subsynchronous operation, as shown in Tables IV and V. Therefore, it is still electromechanical mode but have more participation of electrical states (e'_{ds}, e'_{qs}) than mechanical state (ω_r). The damping of mode# 2 is observed when the controllers are optimized at different wind speeds, as shown in Table VI. It is observed that damping is negative under subsynchronous mode of operation (wind speed is 6 m/s) when controllers are optimized at 8.5 and 8 m/s. However, when optimized at 7.5, 7, and 6.5 m/s, mode# 2 is stable. This confirms that the system stability can be ensured at all wind speeds if the controllers are optimized at any subsynchronous speed.

F. Nonlinear Simulations

The nonlinear simulation of the DFIG system is observed to validate the efficacy of the damping controller and its performance under variable wind speeds. The optimized controller parameters at different wind speeds are used and the system is simulated in MATLAB using ODE15s. The efficacy of the optimization procedure is observed.

The system is subjected to a small perturbation by a small change in the wind speed at 1.0 sec. It amounts to 5% decrease in electrical torque. The system torque returns to its original value after 200 ms. The response of the DFIG system with and without damping controller is shown for supersynchronous and subsynchronous mode of operation in Figs. 5 and 6, respectively. The controller parameters are optimized at $V_w = 7$ m/s. As expected from the eigenvalue analysis, without damping controller, the system is unstable for supersynchronous mode of operation (wind speed is 10 m/s) because of negative damping of mode#3.The system is very well behaved if the optimized damping controller is used. Under subsynchronous mode of operation (wind speed is 6 m/s), the system is stable with and

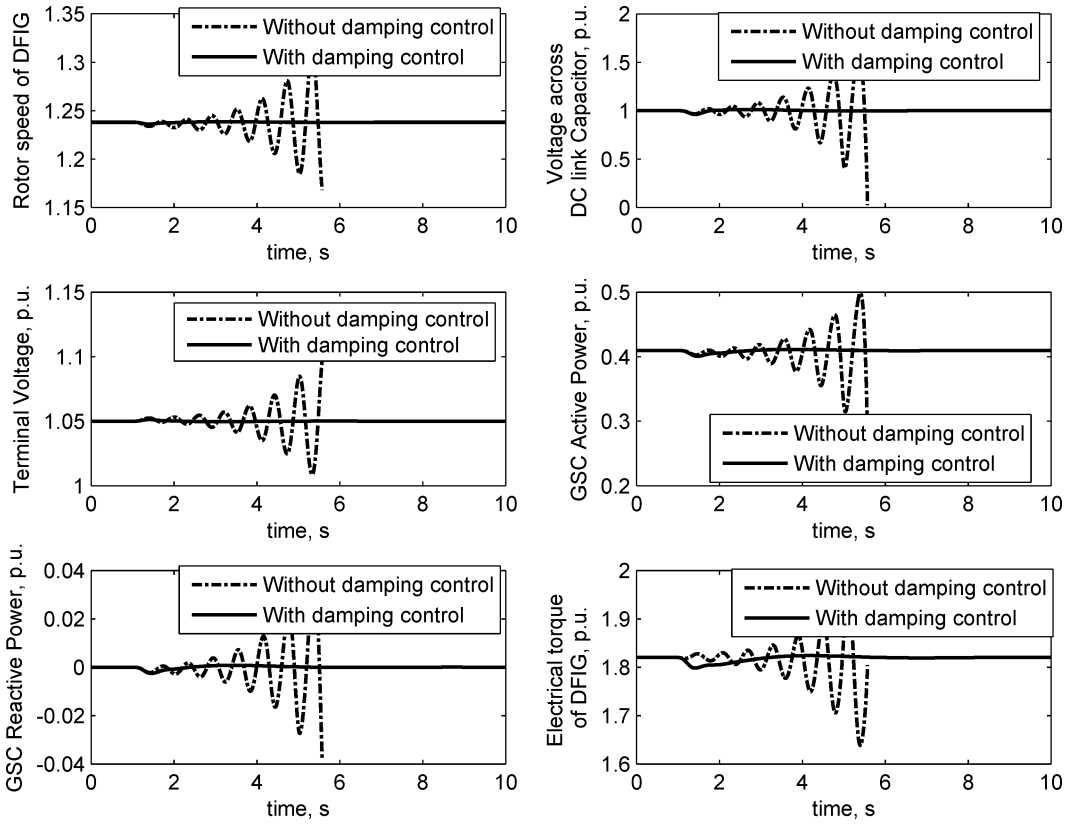

Fig. 5. Dynamic response of the DFIG system when the wind speed is 10 m/s (supersynchronous) and the controllers are optimized at 7 m/s.

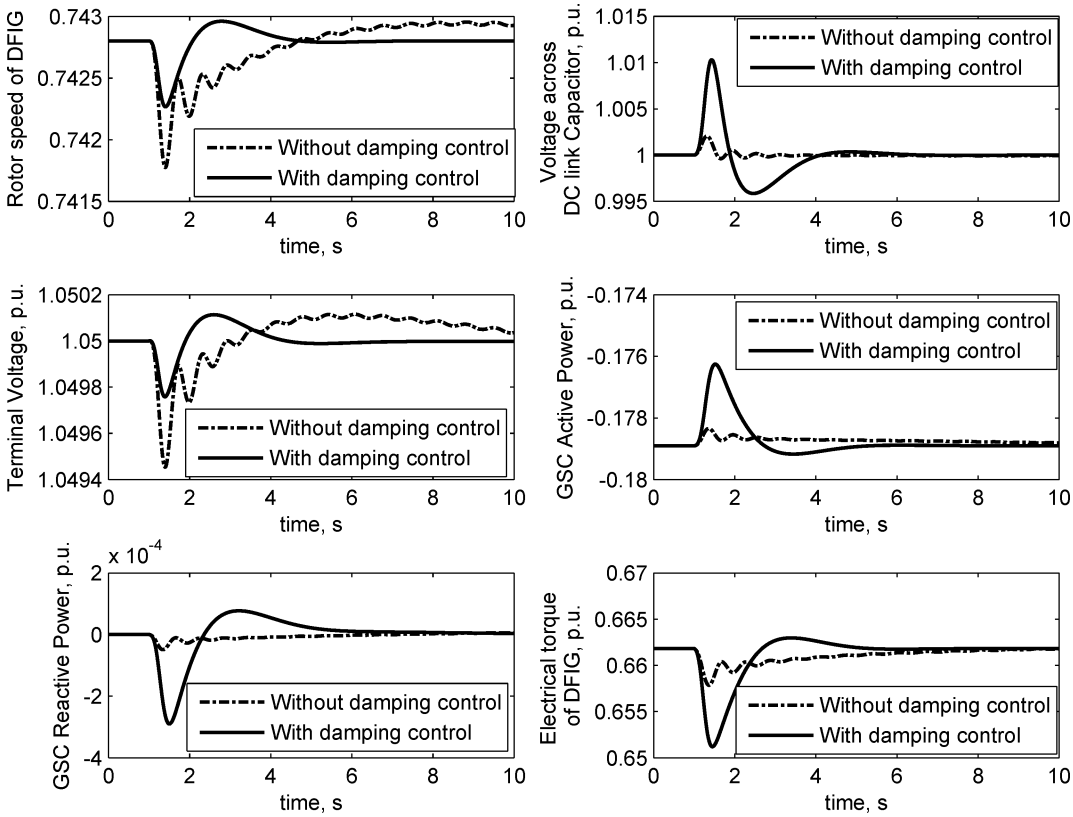

Fig. 6. Dynamic response of the DFIG system when the wind speed is 6 m/s (subsynchronous) and the controllers are optimized at 7 m/s.

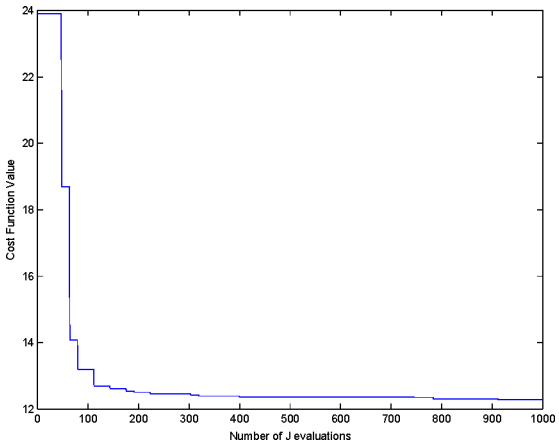

Fig. 7. Performance of BF algorithm for V_w =7.5 m/s.

TABLE VII
OPTIMIZED CONTROLLER PARAMETERS FOR DIFFERENT WIND SPEEDS

speed (m/sec)	K_{Pm} or K_{Im}	m=1 to 7						
		1	2	3	4	5	6	7
8.5	K_{Pm}	.434	.4952	.022	.006	.011	.249	16.11
	K_{Im}	.261	.4632	.171	.159	.236	.123	42.30
8	K_{Pm}	.496	.4949	.48	.496	.468	.275	1.6
	K_{Im}	.105	.447	.384	.440	.249	.179	19.74
7.5	K_{Pm}	.234	.4112	.277	.492	.453	.138	1.285
	K_{Im}	.130	.1657	.181	.451	.358	.073	0.018
7	K_{Pm}	.049	.0017	.022	.493	.159	.446	1.6
	K_{Im}	.122	.1998	.149	.192	.351	.493	2.304
6.5	K_{Pm}	.003	.0015	.089	.21	.013	.082	0.418
	K_{Im}	.044	.3052	.100	.113	.307	.015	0.002

without damping controller. The active and reactive power available at the GSC is also presented. It can be seen that the GSC reactive power variation is well damped. Similar consistent observations are made for other set of wind speeds and optimized controller parameters.

VI. CONCLUSION

The damping controller gives promising results in damping out the low-frequency oscillations and hence improves the system stability of the grid-connected DFIG system. The tuning of the controllers is emphasized to ensure the stable operation under variable wind speed. The supersynchronous, normal, and subsynchronous mode of operation of DFIG-based WT is thoroughly investigated. It is observed that when the tuning of the controllers is done at any subsynchronous speed, the system is stable for all modes of operations. The change in the frequency of the electromechanical modes under super/subsynchronous operation is presented. This study would help in understanding the interaction of the oscillatory modes of DFIG-based WT with other components of power systems. Further, it would also help in proper tuning of the DFIG controllers to enhance the system small-signal stability.

With the increasing penetration of DFIG-based wind farms into the grid, it is important to study the implications of large scale DFIG systems on grid stability. As this study is based on SMIB DFIG system, conclusions of this paper should not be extended to multimachine DFIG-based WT system. Nevertheless, this paper does provide a good initial study of the DFIG system with controller. Computations with multimachine DFIG system will be required to confirm the obtained results and determine if its possible to quantify the impact of DFIGs on power system stability.

APPENDIX

A. Parameters of the SMIB DFIG System (p.u.)

$H_t = 4$; $H_g = 0.4$; $X_m = 4$; $L_m = 4$; $x_{tg} = 0.55$; $C = 0.01$; $x_e = 0.06$; $L_{ss} = 4.04$; $L_{rr} = 4.0602$; $R_s = (X_m/800)$; $R_r = 1.1{*}R_s$.

B. Parameters Used for the Optimization (BF Algorithm)

$S = 4$; $\mathrm{Cl} = 0.07$; $d_{\mathrm{attract}} = 1.9$; $\omega_{\mathrm{attract}} = 0.1$; $h_{\mathrm{repellant}} = d_{\mathrm{attract}}$; $\omega_{\mathrm{repellant}} = 10$.

The earlier values of BF algorithm parameters are used for optimizing the controller parameters. First, all the six controller parameters (i.e., six pairs of K_{Pm} and K_{Im}) are optimized and then the damping controller (K_{P7} and K_{I7}) is optimized for a given wind speed. This process is repeated for different wind speeds. Fig 7 shows the performance of the algorithm for a particular wind speed. Table VII shows the optimized controller parameters using BF algorithm for different wind speeds.

REFERENCES

[1] U.S. Dept. of Energy. (2007, Jun.). EERE state activities and partnerships. [Online]. Available: http://apps1.eere.energy.gov/states/maps/renewable_portfolio_states.cfm

[2] P. B. Eriksen, T. Ackermann, H. Abildgaard, P. Smith, W. Winter, and J. M. R. Garcia, "System operation with high wind penetration," *IEEE Power Energy Manage.*, vol. 3, no. 6, pp. 65–74, Nov. 2005.

[3] W. Qiao, G. K. Venayagamoorthy, and R. G. Harley, "Design of optimal PI controllers for doubly fed induction generators driven by wind turbines using particle swarm optimization," in *Proc. Int. Joint Conf. Neural Netw.*, Canada, Jul. 2006, pp. 1982–1987.

[4] F. Wu, X. P. Zhang, K. Godfrey, and P. Ju, "Small signal stability analysis and optimal control of a wind turbine with doubly fed induction generator," *IET Gener. Transm. Distrib.*, vol. 1, no. 5, pp. 751–760, 2007.

[5] Z. Miao, L. Fan, D. Osborn, and S. Yuvarajan, "Control of DFIG based wind generation to improve inter area oscillation damping," in *Proc. IEEE PES General Meeting*, Pittsburgh, PA, Jul. 2008, pp. 1–7.

[6] L. Fan, Z. Miao, and D. Osborn, "Impact of doubly fed wind turbine generation on inter-area oscillation damping," in *Proc. IEEE PES General Meeting*, Pittsburgh, PA, Jul. 2008, pp. 1–8.

[7] D. J. Vowles, C. Samasinghe, M. J. Gibbard, and G. Ancell, "Effect of wind generation on small signal stability- a New Zealand example," in *Proc. IEEE PES General Meeting*, Pittsburgh, PA, Jul. 2008, pp. 1–8.

[8] F. M. Hughes, O. A. Lara, N. Jenkins, and G. Strbac, "A power system stabilizer for DFIG-based wind generation," *IEEE Trans. Power Syst.*, vol. 21, no. 2, pp. 763–772, May 2006.

[9] F. Mei and B. C. Pal, "Modeling snd small signal analysis of a grid connected doubly fed induction generator," in *Proc. IEEE PES General Meeting*, San Francisco, CA, 2005, pp. 358–367.

[10] S. K. Salman and A. L. J. Teo, "Windmill modeling consideration and factors influencing the stability of a grid-connected wind power based embedded generator," *IEEE Trans. Power Syst.*, vol. 18, no. 2, pp. 793–802, May 2003.

[11] F. Mei and B. C. Pal, "Modal analysis of grid connected doubly fed induction generator," *IEEE Trans. Energy Convers.*, vol. 22, no. 3, pp. 728–736, Sep. 2007.

[12] K. M. Passino, "Biomimicry of bacterial foraging for distributed optimization and control," *IEEE Control Syst. Mag.*, vol. 22, no. 3, pp. 52–67, Jun. 2002.

[13] S. Mishra, "Hybrid least-square adaptive bacteria foraging strategy for harmonic estimation," *IEE Proc.-Gener. Transm. Distrib.*, vol. 152, no. 3, pp. 379–389, May 2005.
[14] M. Tripathy and S. Mishra, "Bacteria foraging-based solution to optimize both real power loss and voltage stability limit," *IEEE Trans. Power Syst.*, vol. 22, no. 1, pp. 240–248, Feb. 2007.
[15] S. Mishra, "A hybrid least square-fuzzy bacteria foraging strategy for harmonic estimation," *IEEE Trans. Evol. Comput.*, vol. 9, no. 1, pp. 61–73, Feb. 2005.
[16] M. Hunjan and G. K. Venayagamoorthy, "Adaptive power system stabilizers using artificial immune system," in *Proc. IEEE Symp. Artif. Life*, Apr. 2007, pp. 440–447.
[17] S. Mishra, M. Tripathy, and J. Nanda, "Multimachine power system stabilizer design by rule based bacteria foraging," *Electr. Power Syst. Res.*, vol. 77, no. 12, pp. 1595–1607, Oct. 2006.
[18] Y. Mishra, S. Mishra, M. Tripathy, N. Senroy, and Z. Y. Dong, "Improving stability of a DFIG-based wind power system with tuned damping controller," *IEEE Trans. Energy Convers.*, vo. 24, no. 3, pp. 650–660, Sep. 2009.

Yateendra Mishra (M'09) received the Ph.D. degree from the University of Queensland, Brisbane, Qld., Australia, in 2009, the B.E. degree from BIT Mesra, Mesra, Ranchi, in 2003, and the M.Tech. degree from Indian Institute of Technology Delhi, New Delhi, India, in 2005.

For six months, he was a Visiting Scholar in the University of Tennessee, Knoxville. He is currently a Transmission Planning Engineer with Midwest ISO, Carmel, IN. His current research interests include distributed generation, doubly fed induction generator (DFIG) based wind generation systems, and power system stability and control.

S. Mishra (M'97–SM'04) received the B.E. degree from the University College of Engineering, Burla, India, in 1990, and the M.E. and Ph.D. degrees from the Regional Engineering College, Rourkela, India, in 1992 and 2000, respectively.

In 1992, he joined the Department of Electrical Engineering, University College of Engineering, as a Lecturer, and subsequently became a Reader in 2001. He is currently an Associate Professor in the Department of Electrical Engineering, Indian Institute of Technology, New Delhi, India. His current research interests include fuzzy logic and artificial neural network applications to power system control and power quality.

Dr. Mishra is a Fellow of the Indian National Academy of Engineering (INAE). He has been honored with many prestigious awards such as the Indian National Science Academy (INSA) Young Scientist Medal-2002, the INAE Young Engineer's Award-2002, the recognition as DST Young Scientist 2001–2002, etc.

Fangxing (Fran) Li (S'98–M'01–SM'05) received the B.S.E.E. and M.S.E.E. degrees from Southeast University, Nanjing, China, in 1994 and 1997, respectively, and the Ph.D. degree from Virginia Tech, Blacksburg, in 2001.

He has been an Assistant Professor at the University of Tennessee (UT), Knoxville, and an Adjunct Researcher at Oak Ridge National Laboratory, since August 2005. He was with ABB, Raleigh, NC, as a Senior and then a Principal Engineer for four and a half years. His current research interests include wind power integration, energy market, reactive power, and distributed energy resources.

Dr. Li is a registered Professional Engineer in North Carolina.

Z. Y. Dong (M'99–SM'06) received the Ph.D. degree from the University of Sydney, Sydney, N.S.W., Australia, in 1999.

He was with the University of Queensland, Australia, and the National University of Singapore. He was also with Powerlink Queensland, and Transend Networks, Tasmania, Australia, both in power system planning area. He is currently with Hong Kong Polytechnic University, Kowloon, Hong Kong. His current research interests include power system planning, power system security, stability, and control, load modeling, electricity market, and computational intelligence and its application in power engineering.

Ramesh C. Bansal (S'99–SM'03) received the M.E. degree from Delhi College of Engineering, New Delhi, India, in 1996, the M.B.A. degree from Indira Gandhi National Open University, New Delhi, in 1997, and the Ph.D. degree from the Indian Institute of Technology Delhi, New Delhi, in 2003.

During June 1999–December 2005, he was an Assistant Professor in the Department of Electrical and Electronics Engineering, Birla Institute of Technology and Science, Pilani, India. During February 2006–June 2008, he was with the School of Electrical and Electronics Engineering Division, School of Engineering and Physics, University of the South Pacific, Suva, Fiji. He was with the Civil Construction Wing, All India Radio, for nine years during August 1989– August 1998. He is currently a Faculty member in the School of Information Technology and Electrical Engineering, the University of Queensland, Brisbane, Qld., Australia. He has authored or coauthored more than 110 papers in national/international journals and conference proceedings. He is a member of the Editorial Board of the Institution of Engineering and Technology (IET), *Renewable Power Generation, Electric Power Components and Systems Energy Sources, Part B: Economics, Planning and Policy*. His current research interests include reactive power control in renewable energy systems and conventional power systems, power system optimization, analysis of induction generators, and artificial intelligence techniques applications in power systems. Dr. Bansal is an Editor of the IEEE TRANSACTIONS OF ENERGY CONVERSION AND POWER ENGINEERING LETTERS, an Associate Editor of the IEEE TRANSACTIONS OF INDUSTRIAL ELECTRONICS. He is a member of the Board of Directors of the International Energy Foundation (IEF), AB, Canada. He is also a member of the Institution of Engineers (India) and a Life Member of the Indian Society of Technical Education.